Lab on a Chip

PAPER

View Article Online
View Journal | View Issue

Cite this: *Lab Chip*, 2016, **16**, 2644

Engineering a perfusable 3D human liver platform from iPS cells†

Arnout Schepers,[ab] Cheri Li,[ab] Arnav Chhabra,[ab] Benjamin Tschudy Seney[ab] and Sangeeta Bhatia*[abcdef]

In vitro models of human tissue are crucial to our ability to study human disease as well as develop safe and effective drug therapies. Models of single organs in static and microfluidic culture have been established and shown utility for modeling some aspects of health and disease; however, these systems lack multi-organ interactions that are critical to some aspects of drug metabolism and toxicity. Thus, as part of a consortium of researchers, we have developed a liver chip that meets the following criteria: (1) employs human iPS cells from a patient of interest, (2) cultures cells in perfusable 3D organoids, and (3) is robust to variations in perfusion rate so as to be compatible in series with other specialized tissue chips (*e.g.* heart, lung). In order to achieve this, we describe methods to form hepatocyte aggregates from primary and iPS-derived cells, alone and in co-culture with support cells. This necessitated a novel culture protocol for the interrupted differentiation of iPS cells that permits their removal from a plated surface and aggregation while maintaining phenotypic hepatic functions. In order to incorporate these 3D aggregates in a perfusable platform, we next encapsulated the cells in a PEG hydrogel to prevent aggregation and overgrowth once on chip. We adapted a C-trap chip architecture from the literature that enabled robust loading with encapsulated organoids and culture over a range of flow rates. Finally, we characterize the liver functions of this iHep organoid chip under perfusion and demonstrate a lifetime of at least 28 days. We envision that such this strategy can be generalized to other microfluidic tissue models and provides an opportunity to query patient-specific liver responses *in vitro*.

Received 5th May 2016,
Accepted 7th June 2016

DOI: 10.1039/c6lc00598e

www.rsc.org/loc

Introduction

The liver is responsible for a multitude of essential functions, including biosynthesis of plasma proteins, energy metabolism, biotransformation of drugs and toxins, and the production of bile.[1,2] The biotransformation of chemicals, which can have both required and/or toxic outcomes in the case of administered drugs, is catalyzed by cytochrome P450 enzymes (CYPs).[3] CYPs are conserved amongst mammals, though the expression of different isoforms, their metabolizing specificity, and products are species-specific.[4,5] These inter-species divergences complicate the extrapolation of animal safety data, resulting in many lead compounds that fail in patients due to either a lack of efficacy or drug-induced toxicity.[6–8] One approach to overcome the cross-species testing divide has been to develop a variety of *in vitro* models of human liver, with the aim to achieve more accurate predictions of potential adverse effects of candidate drugs.[9–11] In some of these efforts, human hepatocytes benefit from co-culture with liver- or non-liver-derived stromal cells in order to retain their phenotypic functions for a period of weeks *in vitro*.[12–17] In addition to determining the cellular makeup of human models, various architectures have been attempted. 3D culture models have the potential to illuminate aspects of biology not observed in 2D; however, dense 3D constructs often suffer from limited nutrient transport, particularly oxygen.[18–38] Continuous media circulation in microfluidic devices can address some of these transport issues, and also offers the possibility to analyze circulation of metabolites to downstream target organs.

Advances in microfabrication techniques have led to several perfused liver models. However, most platforms require complex loading protocols or a period of on chip stabilization,[39–44] which can lead to a high rate of variability

[a] *Koch Institute for Integrative Cancer Research, Massachusetts Institute of Technology, Cambridge, MA 02139, USA. E-mail: sbhatia@mit.edu; Fax: +617 324 0740; Tel: +617 253 0893*
[b] *Institute for Medical Engineering and Science, Massachusetts Institute of Technology, Cambridge, MA 02139, USA*
[c] *Electrical Engineering and Computer Science, Massachusetts Institute of Technology, Cambridge, MA 02139, USA*
[d] *Department of Medicine, Brigham and Women's Hospital and Harvard Medical School, Boston, MA 02115, USA*
[e] *Broad Institute of Massachusetts Institute of Technology and Harvard, Cambridge, MA 02139, USA*
[f] *Howard Hughes Medical Institute, Cambridge, MA 02139, USA*
† Electronic supplementary information (ESI) available. See DOI: 10.1039/c6lc00598e

and limits their scale up. Furthermore, although organ–organ interactions can provide valuable insights in drug toxicity, connecting and scaling different organ modules with different dimensions and flow rates remains problematic.[45] In addition to engineering challenges, finding a robust cell source is essential for reproducing organ specific functions. Functionally, isolated primary human hepatocytes are the cell type of choice for *in vitro* drug metabolism and toxicology assessments.[46,47] However, limited availability of donor material makes it difficult to source enough cells and to examine the effect of genetic polymorphisms in CYP enzymes. The derivation of hepatocytes from iPS cells has been proposed as an unlimited supply of hepatic cells with diverse genetic backgrounds, with the added opportunity to test patient-specific toxicity.[48–51] Currently, iPSC derived hepatocyte-like cells (iHeps) mostly resemble fetal-stage hepatocytes,[52] but additional maturation methods have been described[53–55] and iHeps have been used to successfully predict drug toxicity.[55–57] The combination of organs-on-chips with iPSC technologies will be an important factor for future success.

In this report, we describe a perfused human liver model that is compatible with both primary hepatocytes and iHeps. We phenotypically stabilized primary human hepatocytes by aggregating them with 3T3-J2 fibroblasts in pyramidal microwells.[58,59] Aggregates were encapsulated into small polyethylene glycol (PEG) microtissues,[60,61] which maintained inducible CYP activity. By trapping microtissues in a microfluidic device we were able to provide sufficient transport of oxygen and nutrients to establish albumin secretion for more than 28 days. Microtissues could be cultured under a range of flow rates, providing flexibility for systems integration. In addition, we developed a differentiation protocol to generate functional iHeps in 3D and stabilize them in microtissues. The iHep aggregates are comprised of cells resembling hepatocytes and biliary cells, have inducible CYP activity and show long term function on-chip. This combination provides the opportunity to query patient-specific drug responses.

Experimental

Cell culture and aggregation

Cryopreserved primary human hepatocytes (lot Hu1434 & Hu4175) were obtained from Life technologies. 3T3-J2 murine fibroblasts were a gift from Howard Green of Harvard Medical School[62] and were maintained in DMEM with 10% bovine serum (Invitrogen), 10 U mL^{-1} penicillin, and 10 mg mL^{-1} streptomycin. Cells were cultured in a 5% CO_2 humidified incubator at 37 °C. Hepatocyte culture medium consisted of Dulbecco's Modified Eagle Medium (DMEM; Invitrogen) with 10% fetal bovine serum (Invitrogen), 0.5 U mL^{-1} insulin (Lilly), 7 ng mL^{-1} glucagon (Bedford Laboratories), 7.5 μg mL^{-1} hydrocortisone (Sigma), 10 U mL^{-1} penicillin (Invitrogen), and 10 mg mL^{-1} streptomycin (Invitrogen).

Plates with arrays of square pyramidal microwells, 100 μm or 400 μm side-wall dimension, were fabricated as described previously,[59] or purchased (Aggrewell, Stem Cell Technologies). Pyramidal microwells were pretreated with 5% pluronic F-127 (Sigma); plates were centrifuged at 2000*g* for 5 minutes to remove air bubbles, incubated for 60 minutes and washed twice in DMEM before seeding of cells. All other centrifugation steps were done at 50*g* for 5 min.

iPS cells were differentiated into iHeps according to Si-Tayeb *et al.*[48] with a few adjustments. At day 8 of the differentiation, cells were dissociated using Enzyme free dissociation buffer (Gibco) and aggregated in square pyramidal microwells with 400 μm side-wall dimensions. At day 12, aggregates were encapsulated in PEG-DA hydrogels. At day 22, cells were treated once with 20 μM maturation molecule FH1.[53]

Encapsulation

For microfluidic encapsulation, cell aggregates were pelleted (50*g*, 5 min), and resuspended in PEG-DA pre-polymer. The pre-polymer solution consisted of 100 mg mL^{-1} PEG-diacrylate (20 kDa; Laysan Bio) in heavy DMEM (DMEM adjusted to have a specific gravity of 1.06 by OptiPrep density medium; Sigma) with 1 : 100 v/v photoinitiator (100 mg mL^{-1} Irgacure 2959, Ciba, in *n*-vinyl pyrrolidone; Sigma). The cell suspension was loaded into a syringe and injected into the droplet generator. Simultaneously, Fluorinert® FC-40 (Sigma) containing 0.5% w/v Krytox 157 FSH surfactant (DuPont) was injected into the device as an oil phase. Using a 60 μm nozzle, the aqueous cell suspension was broken into droplets of cells and pre-polymer in oil, which were then continuously polymerized on-chip by exposure to UV light (320–390 nm, 500 mW cm^{-2}, ~0.5 s; Lumen Dynamics) before exiting the device. Polymerized microtissues from the droplet generator were separated from oil and any un-polymerized components by retaining them on a 40 μm cell strainer (BD Falcon) and flushing them with media. After washing, microtissues were collected from the filter and resuspended in hepatocyte medium, and loaded in C-trap microfluidic devices or cultured in 40 μm strainer caps (BD Falcon) as inserts for 24-well plates. C-trap devices were loaded using a 1 ml syringe (BD) with a 23 gauge dispensing needle (McMaster). After trapping the microtissues, the inlet of the device was connected to a media reservoir and the outlet was connected to a peristaltic pump (Ismatec IP-N 24), to pull the media through the device into a collection tube (Fig. S1†).

Device fabrication

Microfluidic devices were designed in AutoCAD. Topographically patterned polydimethylsiloxane (PDMS; Dow Corning) devices were fabricated using standard photolithographic methods. Silicon wafers were spin coated at 1200 rpm with SU-8 2050 photoresist (Microchem) and features were patterned using 50 K DPI photolithography masks (Fineline imaging). Patterned masters were treated with (tridecafluoro-1,1,2,2-tetrahydrooctyl)-1-trichlorosilane (Sigma) for 30 minutes in a vacuum desiccator. PDMS devices were cast from the masters and inlets were made using a 20G needle (McMaster-Carr) before binding the devices to glass

microslides (VWR) by plasma oxidation. Droplet generator devices were coated with Aquapel (PPG Industries) and dried under vacuum prior to use.

Biochemical assays

Secreted albumin in flow-through from the devices was quantified by an enzyme-linked immunosorbent assay (ELISA) kit (Bethyl Labs) according to the manufacturer's instructions. For enzyme induction experiments, microtissues were pretreated with inducers or inhibitors for 72 hours. Stock solutions were prepared in dimethyl sulfoxide (DMSO) and diluted at 1 : 1000 for final concentrations of 50 μM omeprazole (Sigma), 25 μM rifampin (Sigma), 25 μM 8-methoxypsoralen (Sigma), 50 μM quinidine (Sigma), 50 μM ThioTEPA (Sigma). Phenobarbital (Sigma) was dissolved at 40 mM in deionized water and diluted to a final concentration of 1 mM. Vehicle controls were pretreated for 72 hours with DMSO or water. CYP450 activity was assessed by HPLC quantification of metabolites or with luminogenic P450-Glo™ CYP450 assay kits (Promega) according to vendor instructions for non-lytic assays using cultured cells. Processed medium samples were collected from each strainer of microtissues or from flow-through from microfluidic devices and luciferin metabolites were measured on a luminometer (1 s; Tecan).

Immunohistochemistry, live–dead staining, and imaging

Cell viability was examined using calcein AM (5 μg mL^{-1}) and propidium iodide (2 μg mL^{-1}) fluorescent stains (molecular probes; incubated with cells for 30 min, 37 °C) to stain live and dead cells. iHep aggregates were fixed in 4% paraformaldehyde and stained for albumin (Sigma A6684), HNF4α (Santa Cruz sc-8987) and HNF1β (Santa Cruz sc-7411) according to Snippert *et al.*[63] Images were acquired using a Nikon Ellipse TE200 inverted fluorescence microscope and CoolSnap-HQ Digital CCD Camera. ImageJ was used to uniformly adjust brightness/contrast, pseudocolor, and merge images.

Statistical analysis and simulations

Data are presented as mean ± standard deviation. Samples were compared using one-way ANOVA, with p-values of <0.05 considered statistically significant. Statistical significance in figures is represented as follows: $P > 0.05$ = ns, $P \leq 0.05$ = *, $P \leq 0.01$ = **, $P \leq 0.001$ = ***. Theoretical flow profiles were generated using the single-phase laminar flow module on COMSOL Multiphysics. The inputs to the model consisted of a constant fluid velocity at the inlet, zero pressure at the outlet and no-slip boundary condition at the edges. With water implemented as the bulk medium, the shear rate was determined as a function of the distance from each cell-trap and was multiplied by the dynamic viscosity to obtain the shear stress.

Results and discussion

This article presents a microfluidic perfusion system for hepatocyte culture. The design was prompted by the need for a system that cultures cells in perfusable 3D organoids, is robust to variations in perfusion rate and is compatible with iPSC derived hepatocytes.

Hepatocyte aggregation

To model human liver function we aimed to generate a platform as simple, robust, and reproducible as possible. Hepatocytes are the main functional cells of the liver, and previous work has shown that their function can be stabilized *in vitro* by co-culture with supportive stromal cells, *i.e.* murine 3T3-J2 fibroblasts.[14,47] To generate 3D co-cultures, hepatocytes were aggregated with 3T3-J2s (Fig. 1A). Specifically, single cell suspensions with a 3 : 1 ratio of cryopreserved human hepatocytes and 3T3-J2s were seeded into plates with tightly packed square pyramidal microwells with 100 μm side-wall dimensions.[59] Due to the sloping sidewalls of the microwells, centrifugation caused cells to condense at the bottom of the microwells. After condensation, cells were allowed to aggregate for 24 hours. When seeded at a density of ~15 cells per microwell, cryopreserved human hepatocytes co-cultured with 3T3-J2s formed compact aggregates with a diameter of approximately 60 μm (Fig. 1C). In accordance with previous findings from our lab,[58] the aggregation efficiency of hepatocytes cultured without 3T3-J2s was low under these conditions.

Encapsulation of aggregates into microtissues

To avoid uncontrolled growth and aggregation into large structures that would exceed the oxygen and nutrient diffusion limit (Fig. S2†), we proceeded to encapsulate the hepatic aggregates in hydrogel. Hydrogel encapsulation of parenchymal hepatocytes and non-parenchymal cells has been shown to aid in long-term preservation of functionality of hepatic constructs.[17] This step also protects the aggregates from handling associated with loading them on-chip. To generate uniform, non-degradable hydrogels we used PEG-DA, a photopolymerizable macromer which is widely used in tissue engineering due to its non-immunogenicity and resistance to protein absorption.[64] One day after aggregation, aggregates of hepatocytes and fibroblasts were resuspended at a density of 2×10^6 aggregates mL^{-1} in PEG-DA pre-polymer, and injected into a water-in-oil phase droplet generator (Fig. 1B). The droplet size was controlled by changing the ratio between the water and oil phase.[60] Using a flow rate of 800 μl h^{-1} for oil and 200 μl h^{-1} for the cell suspension we generated 100 μm diameter microtissues at ~800 microtissues per minute. Staining with calcein AM and propidium iodide shows that membrane integrity was preserved 24 hours after polymerization of the microtissues (Fig. 1D, Fig. S3†).

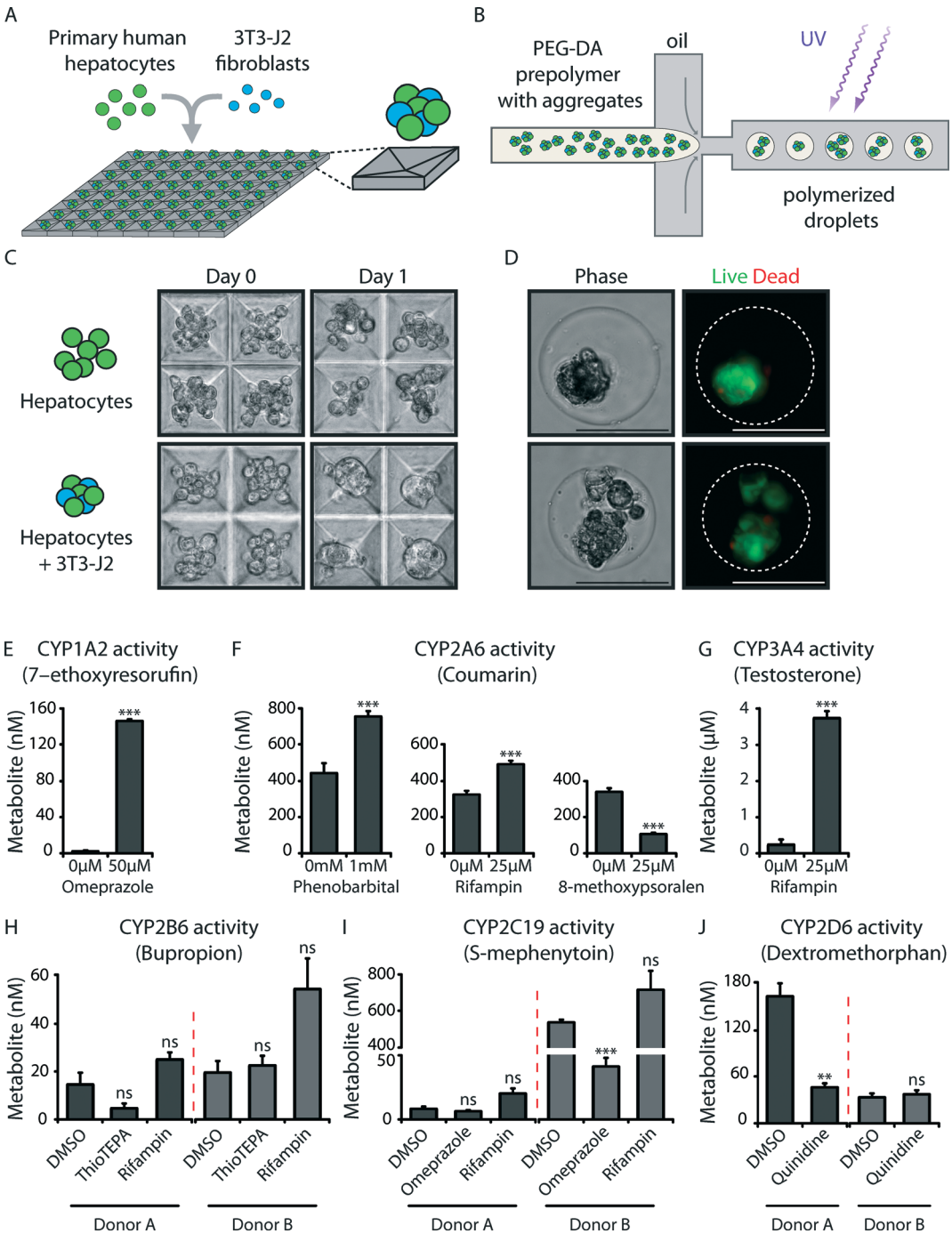

Fig. 1 Fabrication of modular liver microtissues. A) Primary hepatocytes and 3T3-J2 fibroblasts were centrifuged into pyramidal micro-wells (3 : 1 ratio, ~15 cells per pyramid) and allowed to aggregate for 1 day. B) On day 1, cell aggregates were resuspended in PEG-DA pre-polymer, injected into a water-in-oil droplet generator and continuously polymerized on-chip by exposure to a low dose of UV light. C) Hepatocytes alone did not aggregate, whereas co-cultures with 3T3-J2 fibroblasts formed compact aggregates. D) Encapsulated aggregates were tested for viability one day after encapsulation by staining with calcein AM (green; live) and propidium iodide (red; dead). Scale bars represent 100 μm. E–J) Microtissues maintained human specific CYP activity. Microtissues were cultured in strainers and treated with known perturbing agents or control media for 72 hours, starting at day 5 after encapsulation. On day 8, the metabolizing activity was measured by HPLC quantification of metabolites specific for each CYP isoform. Values represent averages of biological triplicates, error bars show standard deviation. E) Cyp1A2 activity evaluated by 7-ethoxyresorufin metabolism, when induced by omeprazole F) Cyp2A6 activity evaluated by coumarin metabolism to coumarin 7-hydroxylase in response to induction by rifampin and phenobarbital, or inhibition by 8-methoxypsoralen. G) Induction of CYP3A4 activity by rifampin using testosterone as a specific substrate. H–J) Comparison of enzyme activity in microtissues generated from two different donors. H) Cyp2B6 activity evaluated by hydroxylation of bupropion in response to inhibition by ThioTEPA or induction by rifampin. I) Cyp2C19 activity evaluated by *S*-mephenytoin metabolism was undetectable in donor A, but could be inhibited by omeprazole or induced by rifampin in donor B. J) CYP2D6 activity evaluated by dextromethorphan could be inhibited by quinidine in donor A, but was not detected in donor B.

Cytochrome P450 enzyme activity of microtissues post-encapsulation

Co-culture can prolong important hepatic functions, *i.e.* CYPs are essential for the biotransformation of many drugs, and their function is rapidly lost when hepatocytes are cultured *in vitro* without stabilization.[65] To assess the functionality of our stabilized human microtissues, we tested the enzymatic activity of prominent CYP isoforms after one week of culture. Microtissues were incubated for 72 hours with selected drugs with established CYP induction or inhibition profiles, and assayed for the presence of drug metabolites in the media. We observed a 350-fold induction of CYP1A2 activity by omeprazole, an AhR (aryl-hydrocarbon receptor) activator (Fig. 1E). Similarly, CYP2A6 was induced by rifampin, a pregnane X receptor (PXR) activator, and by the PXR/constitutive androstane receptor (CAR) activator, phenobarbital. In addition, CYP2A6 activity could be inhibited by 8-methoxypsoralen (Fig. 1F). CYP3A4 is the most abundant isoform of hepatic CYPs, yet levels quickly decrease in *in vitro* culture.[66] In the microtissues, CYP3A4 could be induced by rifampin after one week in culture (Fig. 1G). The ~20-fold induction is consistent with the estimated *in vivo* inducibility reported by Ged *et al.*,[67] where there was an 18-fold increase in CYP3A4 protein levels in liver biopsies after a 4 day rifampin treatment. Genetic polymorphisms in CYP enzymes cause an extensive inter-individual variation in human drug metabolism.[68–70] By using microtissues generated from different hepatocyte donors, we were able to observe patient-specific differences in CYP activity, which may arise from genotypic differences (Fig. 1H–J).

Integrating microtissues on-chip

Continuous media circulation can improve nutrient transport and is essential for multi-organ integration. To perfuse our liver model at different flow rates, we designed a microfluidic device to restrain the microtissues while minimizing shear stress (Fig. 2A). The device contains an array of C-shaped traps, inspired by designs for single cell entrapment,[71,72] and can easily be connected to peristaltic pumps. Theoretical flow profiles were generated to model the media flow in the device (Fig. 2B), and the shear stress was calculated at different points in the device (Fig. 2C). As anticipated, the shear stress is lowest within the traps. The shape and spacing of the traps was optimized to minimize shear stress at physiological flow rates (Fig. 2D), while maximizing the total number of traps in the device. Because the hepatocytes are pre-stabilized in microtissues, they can easily be integrated in the devices without additional cell stabilization on-chip. The devices are optically clear, which allows for easy loading and real-time monitoring. The devices are fabricated out of PDMS, which is permeable to oxygen and gives a sufficient oxygen supply through the device, regardless of the flow rate. Loading the device resulted in an average of 11 microtissues per trap (Fig. 2E). Viability of the microtissues was ~80% upon loading the devices and perfusion culture did not affect the cell health, as measured by AlamarBlue (Fig. S4†). Next, we set out to determine the flexibility of compatible flow rates for our system. The human liver contains about 240 billion cells and receives ~25% of the cardiac output.[73] Using allometric scaling, a cardiac output of ~5 L min^{-1} would translate to a flow rate of ~15 μl h^{-1} for a microliver with 35K cells. However, in multi-organ systems, flow rate adjustments may be required to connect different modules and ensure a suitable physiological contribution to the coupled system. For example flow rates of 20–300 μl h^{-1} have been reported for other organs on-chips containing lung or heart.[74,75] We perfused our microtissues in devices with media at flow rates ranging from 24–540 μl h^{-1} and assessed hepatic function by measuring albumin secretion as a biomarker in the perfusate. Although the shear stress in the C-traps increases linearly with the flow rate (Fig. 2F), we observed no significant difference in albumin levels at different flow rates (Fig. 2G), which provides flexibility to connect our device to other organ modules. Next we set out to determine whether hydrogel encapsulation contributed to protect the aggregates from shear stress. It has been described that perfusion of un-encapsulated hepatocytes entrapped using gravity based aggregation leads to disaggregation of cells from the surface of spheroids.[44] Although our design of the C-traps reduces the shear stress within these structures, the remaining shear stress may still affect the cells. At 540 μl h^{-1}, our model predicts a shear stress up to 0.13 dyn cm^{-2} within the C-traps (Fig. S5†). It has been shown that hepatocytes show reduced functionality under 'high' (5–21 dyn cm^{-2}) *vs.* 'low' shear stress (0.01–0.33 dyn cm^{-2}).[76] Furthermore, perfusion with 0.34 dyn cm^{-2} has been shown to reduce cell adhesion compared to lower shear stress conditions of 0.03 dyn cm^{-2}.[77] To test the importance of encapsulation we loaded our devices with aggregates that were not encapsulated and perfused them at flow rates of 24 and 540 μl h^{-1}. The un-encapsulated aggregates washed out of the C-traps and albumin levels dropped at the higher flow rate of 540 μl h^{-1} (Fig. 2H–I), demonstrating the advantage of encapsulation in our perfusion system. We then looked at long term function by sampling our microtissue-loaded devices every other day. We detected persistent albumin production on-chip for 28 days using microtissues from two different donors (Fig. 2J). Furthermore, coumarin metabolism in perfused devices was higher than in static strainers (Fig. 2K).

Functional iPSC derived hepatocytes on-chip

The development of an *in vitro* platform that depends on access to a limited supply of cadaveric liver cells will still be restricted in its usefulness. To overcome this cell sourcing issue, and to expand the application of our liver model with respect to disease model generation and genotype-specific drug screening, we sought to incorporate iHeps into our platform. Aggregating mature iHeps differentiated using an established four-stage approach[48] was ineffective, as the cells lost their hepatic phenotype upon dissociation, possibly due

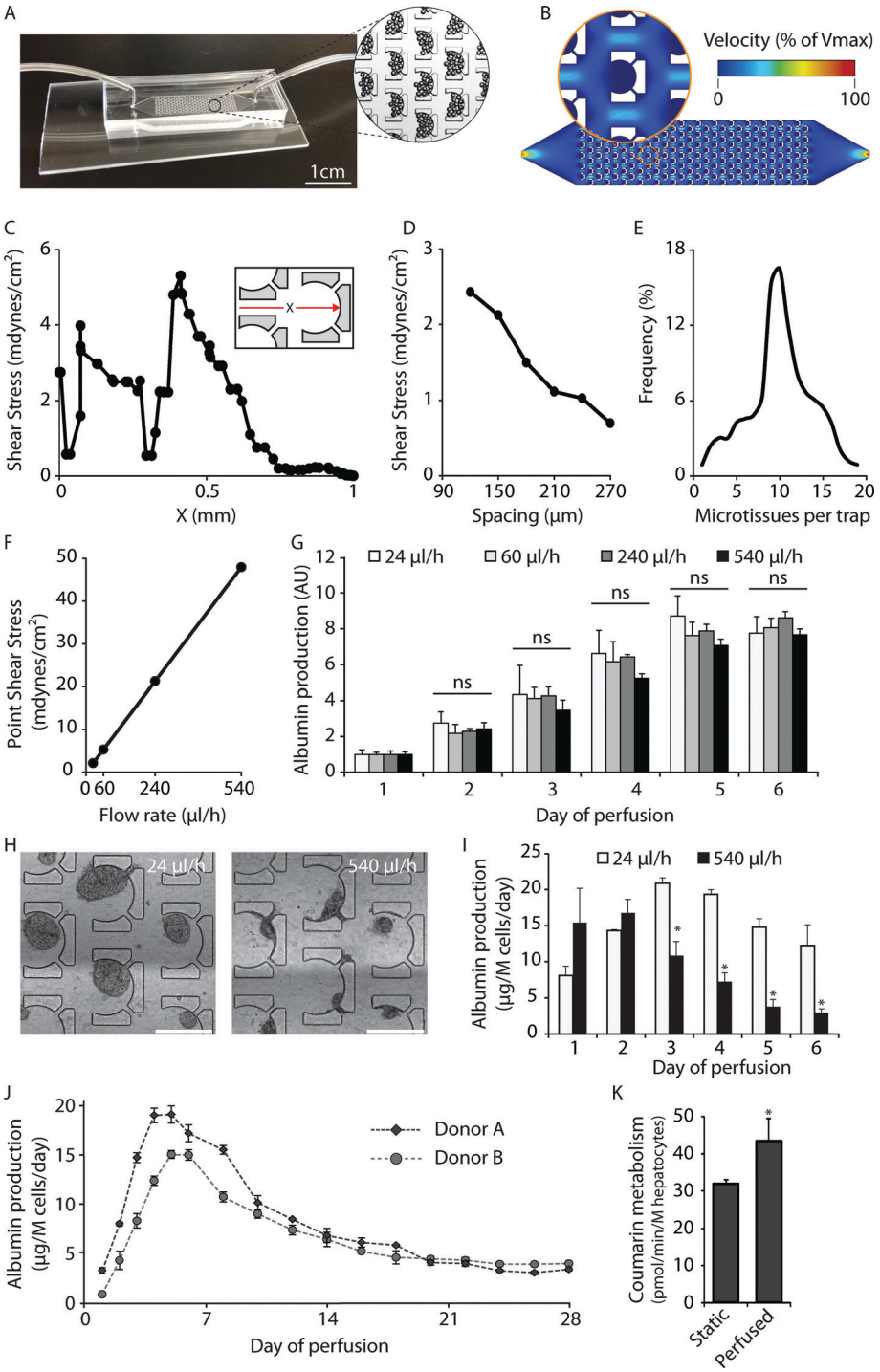

Fig. 2 Integrating microtissues on-chip. A) For on-chip perfusion of microtissues, topographically patterned polydimethylsiloxane devices were designed with trap-like features of 500 μm. Inset shows magnification of traps filled with empty PEG microtissues. B–D) Simulations of fluid flow were conducted for devices bearing traps of varied dimensions and spacing in order to visualize shear-protection offered by the traps in different configurations. C) Shear stress is maximal at the edge of each trap and is significantly less inside the traps. D) Spacing the traps further apart results in lower shear stress forces. E) In the optimal configuration, on average, each trap holds 11 microtissues, with 201 traps per device. F) Simulation of the point shear stress in the device at different flow rates. Shear stress was determined using the product of the shear rate and dynamic viscosity, where shear rate was calculated from the gradient of the velocity vector. G) Microtissues on-chip are functionally stable under different flow rates. Functionality, represented by the total amount of secreted albumin per device per day, was normalized to day 1 values. H–I) Un-encapsulated hepatocyte/3T3-J2 aggregates on chip. Before aggregation, 3T3-J2 cells were growth arrested with mitomycin C (10 μg mL^{-1}, 2 h). Devices were perfused with medium at 24 μl h^{-1} or 540 μl h^{-1}. Bars represent the average albumin levels of three devices. Error bars represent standard error. Images were taken after one week of perfusion. J) Long term on-chip functionality is shown by robust albumin production for 28 days in microtissues derived from two different donors, perfused at 24 μl h^{-1}. K) Rate of coumarin 7-hydroxylation by microtissues cultured in strainers (static) compared to metabolism rate in one pass through an equal amount of microtissues on chip. Values represent averages of biological triplicates, error bars represent standard deviation.

to disrupted cell–cell junctions.[54] To generate 3D cultures with functional iHeps, we interrogated a series of modified differentiation – aggregation – encapsulation protocols,[48,52,54,78] and observed that a brief time window for the transition from 2D to 3D culture was essential for the prolonged functionality of the resulting iHep microtissues (Fig. 3A). Dissociating and aggregating the differentiating cells at a density of ~100 cells per aggregate during the hepatic specification phase yielded functional iHeps in 3D, whereas aggregation during the hepatoblast expansion or hepatic maturation phase yielded microtissues with reduced functionality (Fig. 3B). Hepatic specified iPS cells, dissociated at day 8, formed compact aggregates (Fig. 3C). At day 22 of the differentiation, we confirmed the hepatic identity of cells within the iHep aggregates by positive staining for hepatocyte markers HNF4α and albumin (Fig. 3D). Interestingly, iHep aggregates also contained cells that stained positive for biliary marker HNF1β, indicating that the aggregates represent a mixed population of differentiated cell types. This heterogeneity is also seen in iHeps in 2D culture and in other iPSC

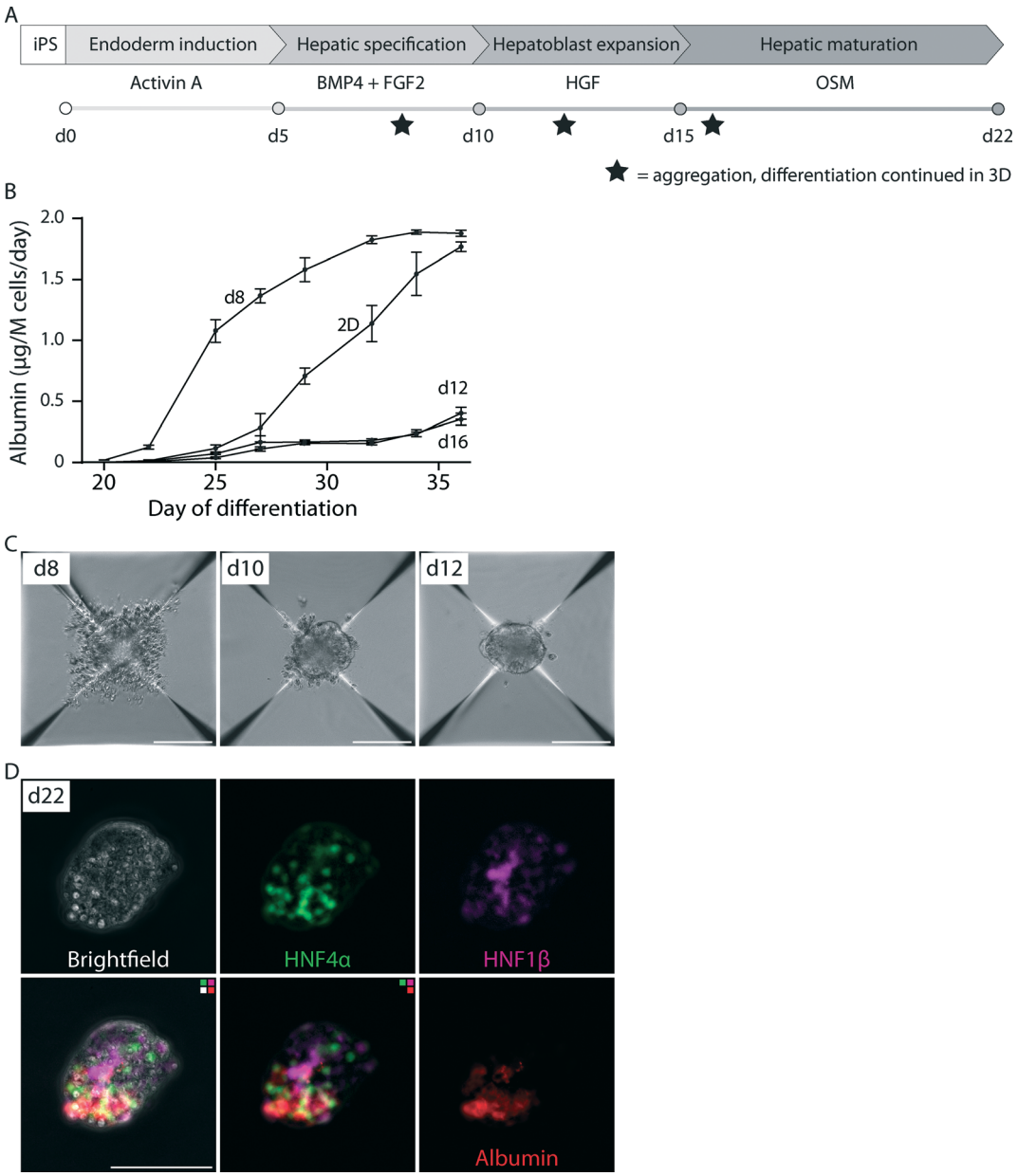

Fig. 3 Differentiation of iPS cells to hepatocytes in 3D. A) Hepatocyte differentiation protocol. Cells were dissociated and aggregated in pyramidal microwells at different days of their differentiation. B) Albumin secretion of the 3D aggregates was compared to the original differentiation protocol in 2D. Lifting cells off and aggregating them during the hepatic specification phase yielded functional iHeps in 3D, whereas aggregation during the hepatoblast expansion or hepatic maturation phase yielded microtissues with reduced functionality. C–D) When dissociated at day 8, hepatic specified iPS cells form compact aggregates in 400 μm aggrewells. D) Aggregates at day 22 of differentiation express markers specific for hepatocytes (HNF4α, albumin) and for bile duct cells (HNF1β). Scale bars in C and D represent 100 μm.

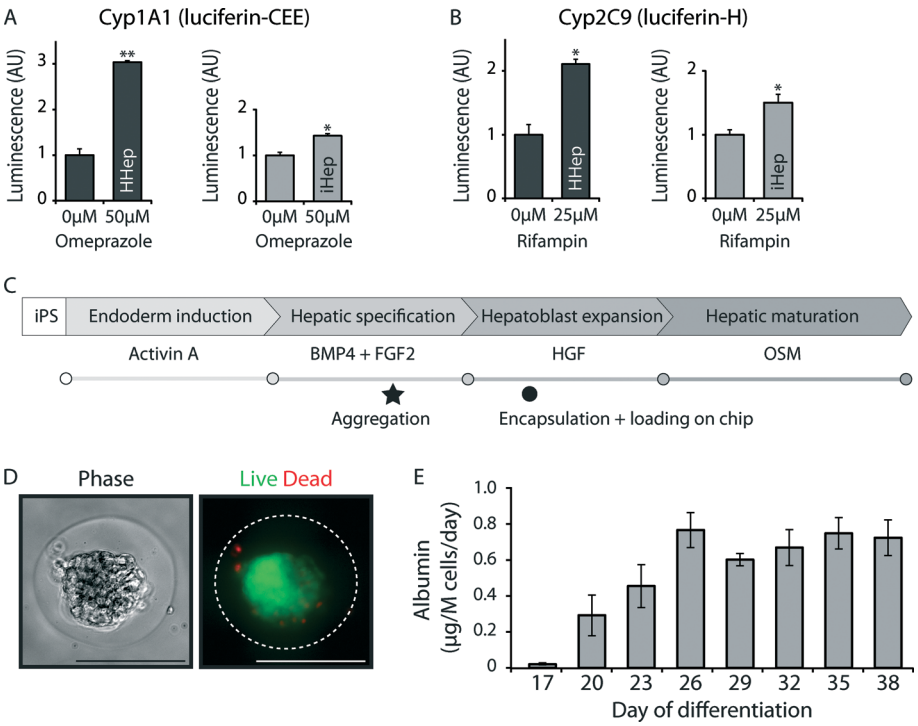

Fig. 4 Functional iPSC derived hepatocytes in 3D. A–B) Inducibility of CYP activity in primary hepatocyte microtissues and in iHep aggregates. Cells were treated with CYP inducers or control media for 72 hours. Microtissues with primary hepatocytes were cultured in strainers, and induction started at day 5 after encapsulation. iHep aggregates were cultured in aggrewells and induction was started at day 19 of the differentiation. CYP activity was evaluated using luminescent substrates specific for either CYP1A1 or CYP2C9. A) CYP1A1 activity, evaluated by luciferin-CEE, could be induced with Omeprazole. B) CYP2C9 activity, evaluated by luciferin-H, could be induced with Rifampin. Values represent averages of biological triplicates, error bars show standard deviation. C) Hepatocyte differentiation protocol. After dissociation and aggregation at day 8, iHep aggregates were encapsulated into PEG-DA hydrogels and trapped in a microfluidic device at day 12 of differentiation. D) Encapsulated iHep aggregates were viable as shown by calcein AM (green; live) and propidium iodide (red; dead). E) Encapsulated iPS derived hepatic microtissues show long term albumin secretion on-chip. Values represent average albumin secretion per day of three different devices, normalized to the amount of cells. Number of cells was estimated based on the number of cells seeded in aggrewells on day 8. Error bars represent standard deviation. Scale bars represent 100 μm.

derived tissues,[48,79,80] where the additional cell types may supplement the roles played by supporting cell types in more systematic co-culture models. Fruitful iHep aggregates that were aggregated at day 8 showed inducible CYP1A1 and CYP2C9 activity at day 22 of their differentiation (Fig. 4A and B). The CYP inducibility was lower than in aggregates comprised of primary hepatocytes, consonant with studies performed in 2D culture.[81] Next we set out to incorporate iHep aggregates on-chip. iHeps continue to proliferate and without encapsulation they eventually overgrew the device (Fig. S2†). To confine their growth, aggregates were encapsulated during the hepatoblast expansion phase (Fig. 4C). This approach yielded viable microtissues (Fig. 4D), which showed robust albumin secretion on-chip for 3 weeks (Fig. 4E).

Conclusions

We have developed a human liver-on-a-chip model compatible with perfusion under a range of flow rates. Co-cultured hepatocytes were encapsulated in hydrogel droplets to form microtissues with stable hepatic function, *e.g.* albumin secretion and metabolic activity. Theoretical modeling was done to design a microfluidic device containing C shaped traps to confine encapsulated microtissues and achieve stable function under a range of flow rates, providing flexibility for integration with other organ modules. On-chip perfusion enabled albumin secretion over 28 days. Aggregation and encapsulation of iPS cells during their differentiation towards hepatocytes yielded microtissues that depicted stable albumin production on-chip and inducible CYP activity, opening the door for patient-specific drug screening.

Acknowledgements

We thank Dr Heather Fleming for critical reading of the manuscript and Stephen Duncan (Medical University of South Carolina) for iPS cell lines. This work was supported by a grant from the National Institutes of Health (UH3 EB017103), and, in part, by the Koch Institute Support (core) Grant P30-CA14051 from the National Cancer Institute. The J2-3T3 fibroblast cell line was kindly provided by Howard Green (Harvard). A. S. is funded by the Dutch Cancer Society. S. N. B. is an HHMI investigator.

References

1 N. J. Hewitt, E. L. Lecluyse and S. S. Ferguson, *Xenobiotica*, 2007, **37**, 1196–1224.
2 S. N. Bhatia, G. H. Underhill, K. S. Zaret and I. J. Fox, *Sci. Transl. Med.*, 2014, **6**, 245sr242.
3 S. A. Wrighton and J. C. Stevens, *Crit. Rev. Toxicol.*, 1992, **22**, 1–21.
4 H. Shih, G. V. Pickwell, D. K. Guenette, B. Bilir and L. C. Quattrochi, *Hum. Exp. Toxicol.*, 1999, **18**, 95–105.
5 M. Martignoni, G. M. Groothuis and R. de Kanter, *Expert Opin. Drug Metab. Toxicol.*, 2006, **2**, 875–894.
6 H. Olson, G. Betton, D. Robinson, K. Thomas, A. Monro, G. Kolaja, P. Lilly, J. Sanders, G. Sipes, W. Bracken, M. Dorato, K. Van Deun, P. Smith, B. Berger and A. Heller, *Regul. Toxicol. Pharmacol.*, 2000, **32**, 56–67.
7 J. F. Pritchard, M. Jurima-Romet, M. L. Reimer, E. Mortimer, B. Rolfe and M. N. Cayen, *Nat. Rev. Drug Discovery*, 2003, **2**, 542–553.
8 J. A. DiMasi, H. G. Grabowski and R. W. Hansen, *N. Engl. J. Med.*, 2015, **372**, 1972.
9 S. A. Wrighton, M. Vandenbranden, J. C. Stevens, L. A. Shipley, B. J. Ring, A. E. Rettie and J. R. Cashman, *Drug Metab. Rev.*, 1993, **25**, 453–484.
10 V. Y. Soldatow, E. L. Lecluyse, L. G. Griffith and I. Rusyn, *Toxicol. Res.*, 2013, **2**, 23–39.
11 S. S. Bale, L. Vernetti, N. Senutosvitch, R. Jindal, M. Hegde, A. Gough, W. J. McCarty, A. Bakan, A. Bhushan, T. Y. Shun, I. Golberg, R. DeBiasio, O. B. Usta, D. L. Taylor and M. L. Yarmush, *Exp. Biol. Med.*, 2014, **239**, 1180–1191.
12 J. Fraczek, J. Bolleyn, T. Vanhaecke, V. Rogiers and M. Vinken, *Arch. Toxicol.*, 2013, **87**, 577–610.
13 J. M. Begue, C. Guguen-Guillouzo, N. Pasdeloup and A. Guillouzo, *Hepatology*, 1984, **4**, 839–842.
14 S. N. Bhatia, U. J. Balis, M. L. Yarmush and M. Toner, *FASEB J.*, 1999, **13**, 1883–1900.
15 A. Guillouzo, *Environ. Health Perspect.*, 1998, **106**(Suppl 2), 511–532.
16 S. R. Khetani, G. Szulgit, J. A. Del Rio, C. Barlow and S. N. Bhatia, *Hepatology*, 2004, **40**, 545–554.
17 M. Yamada, R. Utoh, K. Ohashi, K. Tatsumi, M. Yamato, T. Okano and M. Seki, *Biomaterials*, 2012, **33**, 8304–8315.
18 J. P. Miranda, S. B. Leite, U. Muller-Vieira, A. Rodrigues, M. J. Carrondo and P. M. Alves, *Tissue Eng., Part C*, 2009, **15**, 157–167.
19 C. M. Brophy, J. L. Luebke-Wheeler, B. P. Amiot, H. Khan, R. P. Remmel, P. Rinaldo and S. L. Nyberg, *Hepatology*, 2009, **49**, 578–586.
20 S. J. Griffin and J. B. Houston, *Drug Metab. Dispos.*, 2005, **33**, 115–120.
21 T. Vanhaecke and V. Rogiers, *Methods Mol. Biol.*, 2006, **320**, 209–227.
22 J. C. Dunn, R. G. Tompkins and M. L. Yarmush, *Biotechnol. Prog.*, 1991, **7**, 237–245.
23 L. Richert, D. Binda, G. Hamilton, C. Viollon-Abadie, E. Alexandre, D. Bigot-Lasserre, R. Bars, P. Coassolo and E. LeCluyse, *Toxicol. In Vitro*, 2002, **16**, 89–99.
24 P. V. Moghe, R. N. Coger, M. Toner and M. L. Yarmush, *Biotechnol. Bioeng.*, 1997, **56**, 706–711.
25 F. Berthiaume, P. V. Moghe, M. Toner and M. L. Yarmush, *FASEB J.*, 1996, **10**, 1471–1484.
26 S. Messner, I. Agarkova, W. Moritz and J. M. Kelm, *Arch. Toxicol.*, 2013, **87**, 209–213.
27 R. Glicklis, L. Shapiro, R. Agbaria, J. C. Merchuk and S. Cohen, *Biotechnol. Bioeng.*, 2000, **67**, 344–353.
28 R. Kostadinova, F. Boess, D. Applegate, L. Suter, T. Weiser, T. Singer, B. Naughton and A. Roth, *Toxicol. Appl. Pharmacol.*, 2013, **268**, 1–16.
29 A. Lazar, H. J. Mann, R. P. Remmel, R. A. Shatford, F. B. Cerra and W. S. Hu, *In Vitro Cell. Dev. Biol.: Anim.*, 1995, **31**, 340–346.
30 H. G. Koebe, S. Pahernik, P. Eyer and F. W. Schildberg, *Xenobiotica*, 1994, **24**, 95–107.
31 Y. Nishikawa, Y. Tokusashi, T. Kadohama, H. Nishimori and K. Ogawa, *Exp. Cell Res.*, 1996, **223**, 357–371.
32 F. Pampaloni, E. G. Reynaud and E. H. Stelzer, *Nat. Rev. Mol. Cell Biol.*, 2007, **8**, 839–845.
33 L. G. Griffith and M. A. Swartz, *Nat. Rev. Mol. Cell Biol.*, 2006, **7**, 211–224.
34 S. N. Bhatia and D. E. Ingber, *Nat. Biotechnol.*, 2014, **32**, 760–772.
35 R. Glicklis, J. C. Merchuk and S. Cohen, *Biotechnol. Bioeng.*, 2004, **86**, 672–680.
36 G. Mehta, K. Mehta, D. Sud, J. W. Song, T. Bersano-Begey, N. Futai, Y. S. Heo, M. A. Mycek, J. J. Linderman and S. Takayama, *Biomed. Microdevices*, 2007, **9**, 123–134.
37 G. Catapano, *Int. J. Artif. Organs*, 1996, **19**, 18–35.
38 S. H. Au, M. D. Chamberlain, S. Mahesh, M. V. Sefton and A. R. Wheeler, *Lab Chip*, 2014, **14**, 3290–3299.
39 P. J. Lee, P. J. Hung and L. P. Lee, *Biotechnol. Bioeng.*, 2007, **97**, 1340–1346.
40 Y. C. Toh, C. Zhang, J. Zhang, Y. M. Khong, S. Chang, V. D. Samper, D. van Noort, D. W. Hutmacher and H. Yu, *Lab Chip*, 2007, **7**, 302–309.
41 K. Domansky, W. Inman, J. Serdy, A. Dash, M. H. Lim and L. G. Griffith, *Lab Chip*, 2010, **10**, 51–58.
42 V. N. Goral, Y. C. Hsieh, O. N. Petzold, J. S. Clark, P. K. Yuen and R. A. Faris, *Lab Chip*, 2010, **10**, 3380–3386.
43 M. Hegde, R. Jindal, A. Bhushan, S. S. Bale, W. J. McCarty, I. Golberg, O. B. Usta and M. L. Yarmush, *Lab Chip*, 2014, **14**, 2033–2039.
44 S. A. Lee, D. Y. No, E. Kang, J. Ju, D. S. Kim and S. H. Lee, *Lab Chip*, 2013, **13**, 3529–3537.
45 J. P. Wikswo, E. L. Curtis, Z. E. Eagleton, B. C. Evans, A. Kole, L. H. Hofmeister and W. J. Matloff, *Lab Chip*, 2013, **13**, 3496–3511.
46 P. Godoy, N. J. Hewitt, U. Albrecht, M. E. Andersen, N. Ansari, S. Bhattacharya, J. G. Bode, J. Bolleyn, C. Borner, J. Böttger, A. Braeuning, R. A. Budinsky, B. Burkhardt, N. R. Cameron, G. Camussi, C. S. Cho, Y. J. Choi, J. Craig Rowlands, U. Dahmen, G. Damm, O. Dirsch, M. T. Donato, J. Dong, S. Dooley, D. Drasdo, R. Eakins, K. S. Ferreira, V. Fonsato, J. Fraczek, R. Gebhardt, A. Gibson, M. Glanemann,

C. E. Goldring, M. J. Gómez-Lechón, G. M. Groothuis, L. Gustavsson, C. Guyot, D. Hallifax, S. Hammad, A. Hayward, D. Häussinger, C. Hellerbrand, P. Hewitt, S. Hoehme, H. G. Holzhütter, J. B. Houston, J. Hrach, K. Ito, H. Jaeschke, V. Keitel, J. M. Kelm, B. Kevin Park, C. Kordes, G. A. Kullak-Ublick, E. L. LeCluyse, P. Lu, J. Luebke-Wheeler, A. Lutz, D. J. Maltman, M. Matz-Soja, P. McMullen, I. Merfort, S. Messner, C. Meyer, J. Mwinyi, D. J. Naisbitt, A. K. Nussler, P. Olinga, F. Pampaloni, J. Pi, L. Pluta, S. A. Przyborski, A. Ramachandran, V. Rogiers, C. Rowe, C. Schelcher, K. Schmich, M. Schwarz, B. Singh, E. H. Stelzer, B. Stieger, R. Stöber, Y. Sugiyama, C. Tetta, W. E. Thasler, T. Vanhaecke, M. Vinken, T. S. Weiss, A. Widera, C. G. Woods, J. J. Xu, K. M. Yarborough and J. G. Hengstler, *Arch. Toxicol.*, 2013, **87**, 1315–1530.

47 S. R. Khetani and S. N. Bhatia, *Nat. Biotechnol.*, 2008, **26**, 120–126.

48 K. Si-Tayeb, F. K. Noto, M. Nagaoka, J. Li, M. A. Battle, C. Duris, P. E. North, S. Dalton and S. A. Duncan, *Hepatology*, 2010, **51**, 297–305.

49 Z. Song, J. Cai, Y. Liu, D. Zhao, J. Yong, S. Duo, X. Song, Y. Guo, Y. Zhao, H. Qin, X. Yin, C. Wu, J. Che, S. Lu, M. Ding and H. Deng, *Cell Res.*, 2009, **19**, 1233–1242.

50 X. Ma, Y. Duan, B. Tschudy-Seney, G. Roll, I. S. Behbahan, T. P. Ahuja, V. Tolstikov, C. Wang, J. McGee, S. Khoobyari, J. A. Nolta, H. Willenbring and M. A. Zern, *Stem Cells Transl. Med.*, 2013, **2**, 409–419.

51 H. Inoue, N. Nagata, H. Kurokawa and S. Yamanaka, *EMBO J.*, 2014, **33**, 409–417.

52 R. E. Schwartz, H. E. Fleming, S. R. Khetani and S. N. Bhatia, *Biotechnol. Adv.*, 2014, **32**, 504–513.

53 J. Shan, R. E. Schwartz, N. T. Ross, D. J. Logan, D. Thomas, S. A. Duncan, T. E. North, W. Goessling, A. E. Carpenter and S. N. Bhatia, *Nat. Chem. Biol.*, 2013, **9**, 514–520.

54 R. L. Gieseck, N. R. Hannan, R. Bort, N. A. Hanley, R. A. Drake, G. W. Cameron, T. A. Wynn and L. Vallier, *PLoS One*, 2014, **9**, e86372.

55 D. R. Berger, B. R. Ware, M. D. Davidson, S. R. Allsup and S. R. Khetani, *Hepatology*, 2015, **61**, 1370–1381.

56 K. Takayama, K. Kawabata, Y. Nagamoto, K. Kishimoto, K. Tashiro, F. Sakurai, M. Tachibana, K. Kanda, T. Hayakawa, M. K. Furue and H. Mizuguchi, *Biomaterials*, 2013, **34**, 1781–1789.

57 B. R. Ware, D. R. Berger and S. R. Khetani, *Toxicol. Sci.*, 2015, **145**, 252–262.

58 K. R. Stevens, M. D. Ungrin, R. E. Schwartz, S. Ng, B. Carvalho, K. S. Christine, R. R. Chaturvedi, C. Y. Li, P. W. Zandstra, C. S. Chen and S. N. Bhatia, *Nat. Commun.*, 2013, **4**, 1847.

59 M. D. Ungrin, C. Joshi, A. Nica, C. Bauwens and P. W. Zandstra, *PLoS One*, 2008, **3**, e1565.

60 C. Y. Li, K. R. Stevens, R. E. Schwartz, B. S. Alejandro, J. H. Huang and S. N. Bhatia, *Tissue Eng., Part A*, 2014, **20**, 2200–2212.

61 A. A. Chen, G. H. Underhill and S. N. Bhatia, *Integr. Biol.*, 2010, **2**, 517–527.

62 J. G. Rheinwald and H. Green, *Cell*, 1975, **6**, 331–343.

63 H. J. Snippert, A. G. Schepers, G. Delconte, P. D. Siersema and H. Clevers, *Nat. Protoc.*, 2011, **6**, 1221–1228.

64 J. L. Drury and D. J. Mooney, *Biomaterials*, 2003, **24**, 4337–4351.

65 C. Rodríguez-Antona, M. T. Donato, A. Boobis, R. J. Edwards, P. S. Watts, J. V. Castell and M. J. Gómez-Lechón, *Xenobiotica*, 2002, **32**, 505–520.

66 W. P. Bowen, J. E. Carey, A. Miah, H. F. McMurray, P. W. Munday, R. S. James, R. A. Coleman and A. M. Brown, *Drug Metab. Dispos.*, 2000, **28**, 781–788.

67 C. Ged, J. M. Rouillon, L. Pichard, J. Combalbert, N. Bressot, P. Bories, H. Michel, P. Beaune and P. Maurel, *Br. J. Clin. Pharmacol.*, 1989, **28**, 373–387.

68 S. F. Zhou, J. P. Liu and B. Chowbay, *Drug Metab. Rev.*, 2009, **41**, 89–295.

69 M. Ingelman-Sundberg, S. C. Sim, A. Gomez and C. Rodriguez-Antona, *Pharmacol. Ther.*, 2007, **116**, 496–526.

70 U. M. Zanger, K. Klein, T. Saussele, J. Blievernicht, M. H. Hofmann and M. Schwab, *Pharmacogenomics*, 2007, **8**, 743–759.

71 D. Di Carlo, L. Y. Wu and L. P. Lee, *Lab Chip*, 2006, **6**, 1445–1449.

72 A. M. Skelley, O. Kirak, H. Suh, R. Jaenisch and J. Voldman, *Nat. Methods*, 2009, **6**, 147–152.

73 E. Bianconi, A. Piovesan, F. Facchin, A. Beraudi, R. Casadei, F. Frabetti, L. Vitale, M. C. Pelleri, S. Tassani, F. Piva, S. Perez-Amodio, P. Strippoli and S. Canaider, *Ann. Hum. Biol.*, 2013, **40**, 463–471.

74 D. Huh, B. D. Matthews, A. Mammoto, M. Montoya-Zavala, H. Y. Hsin and D. E. Ingber, *Science*, 2010, **328**, 1662–1668.

75 B. Zhang, M. Montgomery, M. D. Chamberlain, S. Ogawa, A. Korolj, A. Pahnke, L. A. Wells, S. Massé, J. Kim, L. Reis, A. Momen, S. S. Nunes, A. R. Wheeler, K. Nanthakumar, G. Keller, M. V. Sefton and M. Radisic, *Nat. Mater.*, 2016, **15**, 669–678.

76 A. W. Tilles, H. Baskaran, P. Roy, M. L. Yarmush and M. Toner, *Biotechnol. Bioeng.*, 2001, **73**, 379–389.

77 J. K. Noh, J. G. Jung, E. M. Jang, J. H. Lee, H. J. Park, Y. A. Kim, S. M. Jung, C. H. Kwon, D. H. Lee and S. K. Lee, *Transplant. Proc.*, 2012, **44**, 1116–1119.

78 T. Takebe, K. Sekine, M. Enomura, H. Koike, M. Kimura, T. Ogaeri, R. R. Zhang, Y. Ueno, Y. W. Zheng, N. Koike, S. Aoyama, Y. Adachi and H. Taniguchi, *Nature*, 2013, **499**, 481–484.

79 M. Itoh, N. Umegaki-Arao, Z. Guo, L. Liu, C. A. Higgins and A. M. Christiano, *PLoS One*, 2013, **8**, e77673.

80 P. W. Burridge, E. Matsa, P. Shukla, Z. C. Lin, J. M. Churko, A. D. Ebert, F. Lan, S. Diecke, B. Huber, N. M. Mordwinkin, J. R. Plews, O. J. Abilez, B. Cui, J. D. Gold and J. C. Wu, *Nat. Methods*, 2014, **11**, 855–860.

81 Y. Yu, H. Liu, Y. Ikeda, B. P. Amiot, P. Rinaldo, S. A. Duncan and S. L. Nyberg, *Stem Cell Res.*, 2012, **9**, 196–207.

Electronic Supplementary Material (ESI) for Lab on a Chip.

Figure S1. Platform overview
Microtissues consisting of co-cultured hepatocytes or iPSC derived hepatocytes were restrained in a microfluidic device with an array of C-shaped traps. After loading the C-trap devices with microtissues, the inlet of the device was connected to a media reservoir and the outlet was connected to a peristaltic pump to pull the media through the device into a collection tube.

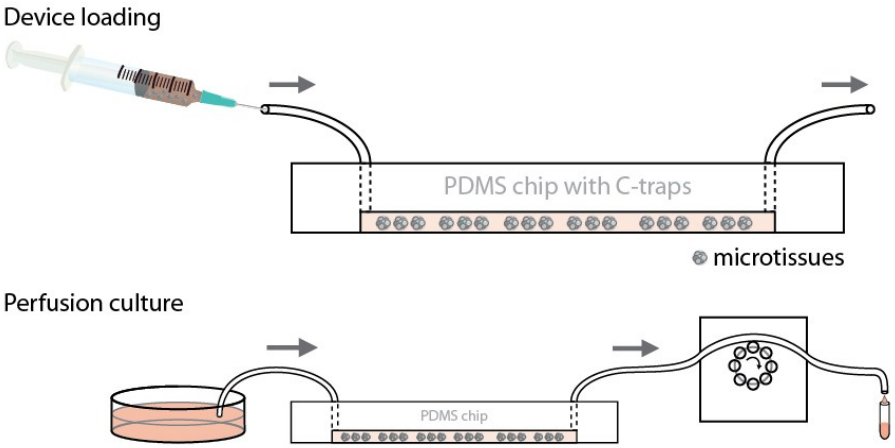

Figure S2. Uncontrolled growth of un-encapsulated aggregates on-chip
A) Aggregates of primary human hepatocytes and 3T3-J2 fibroblasts were loaded on chip and perfused for 28 days. Aggregates clumped together into large structures that exceed the theoretical nutrient diffusion limit with structures as large as 1 mm observed. In addition, fibroblast grew on the inside of the devices despite pretreatment with anti-fouling pluronic (PEG triblock) to reduce cell adhesion. B) iPS cells were dissociated and aggregated at day 8 of their differentiation and loaded on chip at d16. Within four weeks of perfusion, cells had reorganized in the device, increasing the resistance to perfusion. Scale bars represent 500µm.

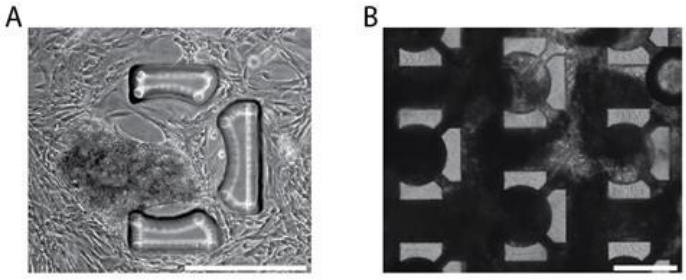

Figure S3. Viability of hepatic aggregates after UV exposure
Hepatic aggregates in aggrewells were exposed to different doses of light at ~365 nm. The UV exposure required to polymerize microtissues (~500 mJ cm^{-2}) did not affect their viability, shown by the percentage of viable cells per aggregate. Three wells with aggregates were exposed per condition, and analyzed 24 and 48 hours after exposure. Viability was analyzed by Calcein AM (live) and Propidium Iodide (dead). The number of Calcein positive cells is represented as a percentage of total number of cells. Error bars represent standard deviation.

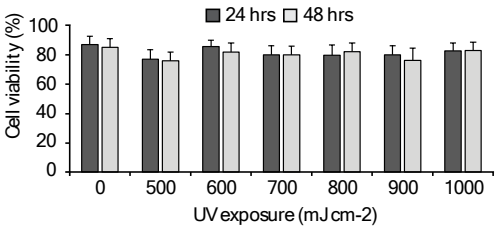

Figure S4. Viability of hepatic microtissues under perfusion

Cell viability was evaluated during perfusion culture by AlamarBlue assay (ThermoFischer). Microfluidic devices, perfused at 24µl/h, were disconnected from the pump, injected with 50 µl of 1x AlamarBlue reagent in ITS media, and incubated for 1 hour without perfusion. After incubation, samples were collected at the outlet by injecting 50 µl of ITS media to the inlet, and devices were reconnected to the pump. Samples were transferred to a 96 well plate and fluorescence was measured in a microplate reader (Tecan). Fluorescent spectra were normalized to day 4 values. Bars represent the average measurement from three different devices. Error bars represent standard deviation.

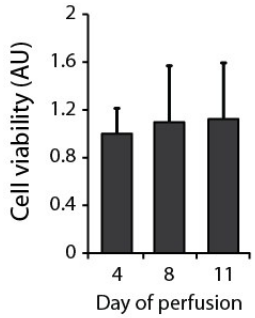

Figure S5. Shear stress modeling

Shear stress was modeled for a flow rate of 540µl/h along five different streamlines in the device using Comsol Multiphysics.